



## ARTICLE

# Rituximab pharmacokinetic and pharmacokinetic–pharmacodynamic evaluation based on a study in diffuse large B-cell lymphoma: Influence of tumor size on pharmacokinetic and assessment of pharmacokinetic similarity

Robin J. Svensson<sup>1</sup> | Qing Xi Ooi<sup>1</sup> | Lena E. Friberg<sup>1,2</sup> | Narendra Maharaj<sup>3</sup> | Pramod Kumar Reddy<sup>3</sup> | Luis López-Lázaro<sup>4</sup> | Emma Hansson<sup>1</sup>

<sup>1</sup>Pharmetheus AB, Uppsala, Sweden

<sup>2</sup>Department of Pharmacy, Uppsala University, Uppsala, Sweden

<sup>3</sup>Dr. Reddy's Laboratories Ltd, Hyderabad, Telangana, India

<sup>4</sup>Dr. Reddy's Laboratories SA, Basel, Switzerland

## Correspondence

Pramod Kumar Reddy, Dr. Reddy's Laboratories Ltd, Hyderabad, Telangana, India.

Email: [pramodkrp@drreddys.com](mailto:pramodkrp@drreddys.com)

Luis López-Lázaro, Dr. Reddy's Laboratories SA, Elisabethenanlage 11, CH-4051 Basel, Switzerland.

Email: [llopezlazaro@drreddys.com](mailto:llopezlazaro@drreddys.com)

## Abstract

Dr. Reddy's Laboratories rituximab (DRL\_RI; Dr. Reddy's Laboratories SA, Basel, Switzerland) is under development as a rituximab biosimilar. Study RI-01-002 (Clinical Trials Registry - India/2012/11/003129), comparing DRL\_RI to the reference medicinal product (RMP) MabThera® (Roche, Grenzach-Wyhlen, Germany), demonstrated pharmacokinetic (PK) equivalence and showed comparable pharmacodynamic, efficacy, safety, and immunogenicity profiles. We used data from the same study to perform population PK and PK–pharmacodynamic analyses: first exploring possible factors influencing the PK similarity assessment between products and then performing simulations to investigate the impact of tumor size on rituximab PK. Nonlinear mixed-effects models for PK, tumor size, tumor size–PK, and tumor response were developed independently. The final PK model included drug product as a dose-scaling parameter and predicted a 6.75% higher dose reaching the system in RMP-treated patients. However, when tumor size was included in the tumor size–PK model, the drug product effect was no longer observed. The model rather indicated that patients with larger tumor size have higher clearance. Further simulations confirmed that higher baseline tumor size is associated to slightly lower rituximab exposure. Tumor response, described by a continuous-time Markov model, did not differ between drug products. Both had higher effects during the first 20 weeks of treatment. Also, the model described a subpopulation of nonresponders to treatment (42%) with faster transitions to a worse state. The different rituximab exposure initially detected between drug products (6.75%) was shown using PK/PK–pharmacodynamic analysis to be attributed to a tumor size imbalance

Luis López-Lázaro and Emma Hansson contributed equally.

This is an open access article under the terms of the [Creative Commons Attribution-NonCommercial-NoDerivs](https://creativecommons.org/licenses/by-nc-nd/4.0/) License, which permits use and distribution in any medium, provided the original work is properly cited, the use is non-commercial and no modifications or adaptations are made.

© 2022 Dr. Reddy's Laboratories SA. *CPT: Pharmacometrics & Systems Pharmacology* published by Wiley Periodicals LLC on behalf of American Society for Clinical Pharmacology and Therapeutics.

between treatment groups. PK/PK-pharmacodynamic analyses may contribute to PK similarity assessments.

### Study Highlights

#### WHAT IS THE CURRENT KNOWLEDGE ON THE TOPIC?

There is an urgent need to develop rituximab biosimilars to enable patient access to quality and affordable treatments.

#### WHAT QUESTION DID THIS STUDY ADDRESS?

Do the pharmacokinetic (PK) and PK-pharmacodynamic profiles of rituximab differ between the two drug products here compared, Dr. Reddy's Laboratories rituximab and the reference medicinal product? What is the impact of tumor size on rituximab PK profiles?

#### WHAT DOES THIS STUDY ADD TO OUR KNOWLEDGE?

The drug product was not a significant predictor of PK, tumor size, or tumor response. Larger tumor size is associated to slightly lower rituximab exposure.

#### HOW MIGHT THIS CHANGE DRUG DISCOVERY, DEVELOPMENT, AND/OR THERAPEUTICS?

Population PK-pharmacodynamic analyses may contribute to PK similarity assessments by evaluating specific issues observed in the studies. Despite the current regulations for biosimilarity assessments limiting the use of population analysis for this scope, the current analysis is an example of how such a study can identify hidden factors generating apparent differences between drug products.

## INTRODUCTION

Rituximab is a chimeric anti-CD20 monoclonal antibody used to treat various autoimmune diseases and cancer forms. Rituximab binds to CD20, mainly present on B cells, and kills both normal and malignant CD20<sup>+</sup> cells via multiple mechanisms. Rituximab has been proved effective in patients with various lymphoid malignancies, including non-Hodgkin lymphomas (NHL).<sup>1,2</sup> Diffuse large B-cell lymphoma (DLBCL) is the most common histological type of NHL, comprising up to 40% of all cases globally.<sup>3</sup> It is a heterogeneous, fast-growing, and aggressive form of lymphoma and is known to have the highest expression of cell-surface CD20 compared with other B-cell malignancies.<sup>4,5</sup> In patients suffering from DLBCL, long-term outcomes have significantly improved after the addition of rituximab to the standard-of-care chemotherapy cyclophosphamide, doxorubicin, vincristine, and prednisone (CHOP).<sup>6,7</sup> The high costs of rituximab necessitate the urgent development of new biosimilars to allow more patients access to safe and affordable treatment.<sup>8,9</sup>

Dr. Reddy's Laboratories rituximab (DRL\_RI; Dr. Reddy's Laboratories SA, Basel, Switzerland) is under development as a rituximab biosimilar and has been

compared with the EU and US reference medicinal product (RMP; MabThera<sup>®</sup>, Roche, Grenzach-Wyhlen, Germany).<sup>10,11</sup> The results of study RI-01-002 (Clinical Trials Registry - India/2012/11/003129) demonstrated pharmacokinetic (PK) equivalence between DRL\_RI and RMP and showed comparable pharmacodynamic, efficacy, safety, and immunogenicity profiles.<sup>10</sup> This study was powered for demonstrating PK similarity but not similarity in efficacy/pharmacodynamics. Previous knowledge shows that rituximab undergoes target-mediated drug disposition (TMDD),<sup>12</sup> thus determining a reciprocal dependence of PK and pharmacodynamics profiles. Understanding these drug characteristics may facilitate results interpretation. Therefore, population PK and PK-pharmacodynamic analyses were conducted to aid the evaluation of PK similarity between DRL\_RI and RMP. Specifically, these analyses aimed to identify and explain any differences in PK and/or pharmacodynamic between drug products and to characterize the exposure-response for selected end points. The population PK and PK-pharmacodynamic profiles of rituximab were characterized for several end points, with the aims to (i) explore factors influencing the PK similarity assessment of the two products and (ii) perform simulations to explore the impact of tumor size on rituximab PK.

## METHODS

### Study design

The population PK and PK–pharmacodynamic analyses were based on data from study RI-01-002,<sup>10</sup> a randomized, double-blind, parallel-group clinical study conducted in 151 patients with DLBCL at 44 centers in India. Patients were aged 18 to 60 years, previously untreated, and had histologically confirmed CD20-positive disease (Tables S2, S3). Patients were randomly assigned to either of the two treatment arms: DRL\_RI ( $n = 76$ ) and RMP ( $n = 75$ ). In both arms, patients received rituximab at the approved doses of 375 mg/m<sup>2</sup> body surface area (BSA) as a 4-h intravenous infusion on Day 1 of each 21-day rituximab-CHOP cycle, for a total of six cycles (Figure S1).<sup>10</sup> The Supplementary Material includes details on sampling schedules for PK and pharmacodynamic end points (Figure S1), study design, and analytical assessments (Methods S1). The study was approved by an independent ethics committee or institutional review board at each study center and conducted in accordance with the Declaration of Helsinki, International Council for Harmonization Good Clinical Practice guidelines, and applicable local regulations. Each patient provided written informed consent before study entry.

### Model development

Nonlinear mixed-effects models for PK, tumor size, tumor size–PK, and tumor response were developed independently. Three more end points (dropout, event-free survival, and B-cell counts) were modeled in this analysis but, for parsimony, will not be presented here. The relationship between PK and B-cell counts was explored but was not carried forward due to limited improvement in model fit and model instability. Furthermore, informative dropout was accounted for when evaluating the tumor size model using visual predictive checks (VPCs).

In the PK–pharmacodynamic analyses of tumor size and tumor response, the individual PK parameters (IPP) approach<sup>13</sup> was used to predict the continuous rituximab concentrations using the final intermediate PK model.

### Structural model

#### Intermediate PK model

The starting point for the PK analysis was a rituximab PK model previously described in DLBCL patients:<sup>14</sup> a linear two-compartment model where BSA was included

as a covariate on central volume of distribution ( $V_c$ ). This model<sup>14</sup> was first evaluated with the PK data from study RI-01-002 (in NONMEM with MAXEVAL = 0 and a VPC), then reestimated based on data from the same study, and finally adjusted to describe the current data. Among other adjustments, BSA was removed from the model and only body weight (WT) was included as a time-varying structural covariate using allometric scaling with estimated exponents on clearance and volume of distribution terms. At this stage, the analysis indicated model misspecifications that could be possibly due to TMDD.<sup>12</sup> Therefore, a TMDD model<sup>15</sup> with a quasi-equilibrium (QE) assumption<sup>16</sup> was implemented assuming a 1:1 binding proportion between rituximab and the receptor (Results S1). The TMDD model assumed that the target was present in the central compartment and the free drug concentrations measured by the PK assay were predicted by subtracting the total complex concentrations from the total drug concentrations. The model obtained was used for the covariate analysis step (Table S1) and thereafter considered as the final intermediate PK model.

#### Tumor size model

Tumor size was assessed as the sum of products of diameters (SPD) for target lesions. To develop the tumor size model, two starting points were considered: the Claret et al. 2009 model<sup>17</sup> and the Stein et al. 2008 model.<sup>18</sup> The first model had stability issues and was not taken forward; therefore, the Stein et al. 2008 model was used. Equations were further adapted by adding the parameter Base to describe complete response (CR), which in DLBCL is defined as the lymph node returning to the normal/healthy size:

$$\text{SPD} = \text{TUM}_0 \cdot (1 - p_{\text{resistant}}) \cdot e^{-k_{\text{kill}} \cdot \text{TSFD}} + \text{TUM}_0 \cdot p_{\text{resistant}} \cdot e^{k_g \cdot \text{TSFD}} + \text{Base}, \quad (1)$$

where TSFD is the time since first dose,  $\text{TUM}_0$  is the parameter describing the estimated baseline tumor size,  $k_{\text{kill}}$  is a first-order net kill rate constant for the susceptible tumor fraction,  $k_g$  is a first-order tumor growth rate constant, and  $p_{\text{resistant}}$  is the fraction of the tumor nonsusceptible to treatment described as

$$p_{\text{resistant}} = \frac{e^{\theta_{\text{TUM, resistant}}}}{1 + e^{\theta_{\text{TUM, resistant}}}}, \quad (2)$$

where  $\theta_{\text{TUM, resistant}}$  is the logit of  $p_{\text{resistant}}$ . The number of target lesions (NTARG) was explored on  $\theta_{\text{Base}}$  as a structural, time-varying covariate using the power model:

$$\text{Base} = \theta_{\text{Base}} \cdot \left( \frac{\text{NTARG}}{3} \right)^{\theta_{\text{NTARG-base}}}, \quad (3)$$

where  $\theta_{\text{NTARG-base}}$  is a coefficient for number of target lesions on  $\theta_{\text{Base}}$ . The maximum number of target lesions observed was nine. To account for tumor regrowth in a fraction of patients, two subpopulations of  $k_g$  were specified: one with  $k_g$  of 0 and another for which  $k_g$  was estimated. The addition of exposure–response of rituximab on  $k_{\text{kill}}$ , using the maximum effect ( $E_{\text{max}}$ ) function, did not improve the model and was thus not taken further. Thus, the model here described was used for the covariate analysis step.

## Tumor size–PK model

A tumor size–PK model was then developed and used to investigate the impact of tumor size on rituximab total clearance. The intermediate PK model, used as starting model, was modified by (a) removing the drug product scaling effect on the rituximab dose (identified as a covariate), (b) removing the TMDD model<sup>15</sup> with a QE assumption,<sup>16</sup> and (c) introducing a saturable elimination pathway where rituximab clearance (CL) was described by

$$\text{CL}(t) = \text{CL} + \frac{V_{\text{max}}}{K_m + C_p}, \quad (4)$$

where CL represents a constant CL term,  $V_{\text{max}}$  is the maximum elimination capacity,  $K_m$  is the concentration at half maximum elimination capacity, and  $C_p$  is the predicted rituximab plasma concentration. The individual, time-varying tumor size (predicted by the final tumor size model using the IPP approach) was then explored on  $V_{\text{max}}$  with a power relationship. Furthermore, assuming that  $K_m \gg C_p$  and that  $K_m + C_p \approx K_m$ ,  $C_p$  was removed from the tumor size–dependent component of CL and  $\frac{V_{\text{max}}}{K_m}$  was simplified to  $\text{CL}_{\text{TS}}$ , leading to a good model fit.

## Tumor response model

The continuous time Markov model (CTMM), which has been previously applied to model other ordered categorical end points,<sup>19–24</sup> was used to model the tumor response data. The categories included were the following: CR, partial response (PR), stable disease (SD), progressive disease (PD), and dropout (DO). The response category definitions,<sup>25</sup> the CTMM implemented in the current analysis, and the related equations are reported as Supplementary Material (Methods S1).

Individually predicted drug exposure derived using the IPP approach based on the final intermediate PK model and TSFD were considered as structural covariates. Adding exposure–response using the additive or proportional linear,  $E_{\text{max}}$ , sigmoid  $E_{\text{max}}$ , and power models on the rate constants

between categories ( $k_{\text{SD-PR}}$  and  $k_{\text{PR-CR}}$ ) did not significantly improve the model. The effect of TSFD ( $E_{\text{TSFD}}$ ) was tested on  $k_{\text{SD-PR}}$  and  $k_{\text{PR-CR}}$  using the exponential model and the sigmoid time to  $E_{\text{max}}$  model. To allow for maximum flexibility, the rate constants were assumed to consist of two parts:  $k_{i-j,\text{TSFD}}$ , dependent on TSFD, and  $k_{i-j}$ , time independent.

$$k_{i-j,\text{effective}} = k_{i-j} + k_{i-j,\text{TSFD}} \cdot E_{\text{TSFD}} \quad (5)$$

Finally, a mixture model on  $k_{\text{CR-PR}}$ ,  $k_{\text{PR-SD}}$ , and  $k_{\text{SD-PD}}$  was tested and assumed that the population who did not respond to treatment had higher values for all of these transfer-rate constants compared with the population who responded to treatment. This base model was further used for the covariate analysis step.

## Stochastic model

For the PK model, the interindividual variabilities (IIVs) initially considered were on CL,  $V_c$ , intercompartmental clearance (Q), and peripheral volume of distribution ( $V_p$ ). Furthermore, IIVs were tested on dissociation constant, baseline amount of target/receptors ( $R_{\text{tot},0}$ ), and TMDD-related CL parameters. For the tumor size model, IIVs were tested on  $\theta_{\text{Base}}$  and  $k_g$ . For the tumor response model, IIVs were tested on the rate constants, either taken alone or together, with and without the correlation terms.

Residual unexplained variability (RUV) was included in the PK model and the tumor size models as a log-additive (exponential) error model.

## Covariate model

Missing covariates were imputed with the median (for continuous covariates) or most common category (for categorical covariates) in the data set. If a patient missed one, or more, values for a time-varying covariate, these were imputed by carrying forward the closest previous value.

Various baseline covariates (Table S1) were tested using the stepwise covariate model building procedure (SCM)<sup>26–29</sup> (Methods S1).

For all primary models (intermediate PK, tumor size, and tumor response models), after completion of the first SCM testing exploratory covariates, a second SCM was conducted to specifically test the effects of drug product (DRL\_RI or RMP). For the tumor size–PK model, no exploratory covariate analysis was conducted, but the effects of drug product were tested. Covariates that were not deemed clinically relevant were removed from the final model.

## Model evaluation

For modeling of continuous end points (i.e., PK, tumor size), model evaluation was based on graphical inspection of goodness-of-fit (GOF) plots, relative standard errors (RSEs) of parameters, and VPCs (Methods S1). For the tumor response end point, model evaluation was mainly based on RSEs and VPCs. Dropout was accounted for when generating VPCs for the tumor size model. The detailed methods used for model discrimination and finalization are described in Methods S1.

## Simulations

Simulations were performed to evaluate the impact of baseline tumor size on rituximab PK (conditions used for the simulations are described in Methods S1). All parameters from the final tumor size–PK model, except  $TUM_0$ , were used to simulate longitudinal tumor sizes and exposures. Conversely,  $TUM_0$  was considered according to three possible scenarios based on the median and percentiles of the observed baseline tumor size across all patients:

Low tumor size scenario:  $TUM_0$  set to  $1070\text{ mm}^2$  (i.e., 25th percentile).

Median tumor size scenario:  $TUM_0$  set to  $2615\text{ mm}^2$  (i.e., median).

High tumor size scenario:  $TUM_0$  set to  $4681\text{ mm}^2$  (i.e., 75th percentile).

Two more scenarios, considering tumor size and treatment arm, were explored but did not indicate significant results (Methods S1). The three scenarios mentioned previously were simulated to generate the following model-based secondary parameters: area under the curve over the dosing interval ( $AUC_{0-21}$ ), maximum concentration ( $C_{max}$ ), and trough concentration ( $C_{tr}$ ). These secondary parameters were summarized in Cycles 1 and 6 using boxplots.

## Software and hardware

Model development was conducted using NONMEM (Version 7.3; ICON plc).<sup>30</sup> The first-order conditional estimation method with interaction was used for modeling PK and tumor size. For the CTMM, the Laplacian estimation method in NONMEM was used. Perl-speaks-NONMEM Version 4.9.0<sup>26–28</sup> was used for automation and postprocessing purposes. The software R (Version 3.5.3; R Foundation for Statistical Computing)<sup>31</sup> was used for data management. R, including the package xpose4 Version 4.6.1,<sup>28,32</sup> was used for GOF analyses and model evaluation.

## RESULTS

### Patient demographics and clinical data

Patient demographics (Tables S2, S3) were largely similar between drug products, except for baseline tumor size that was slightly higher for the DRL-RI treatment. In total, 3914 PK samples were collected from 151 patients, 1010 tumor size observations were recorded from 141 patients, and 1003 tumor response observations were recorded from 144 patients. The number of observations and patients were almost equally distributed between DRL-RI and RMP treatments.

### Graphical analysis

After rituximab administration, a biphasic distribution pattern was observed, suggesting that a two-compartment disposition model was needed to describe the PK of rituximab (Figure 1a). No strong signs of TMDD were observed. Both drug products appeared to have comparable PK profiles. Also, no differences were observed in the PK profiles of the five subjects with antidrug antibodies (ADA) positivity included in the study.

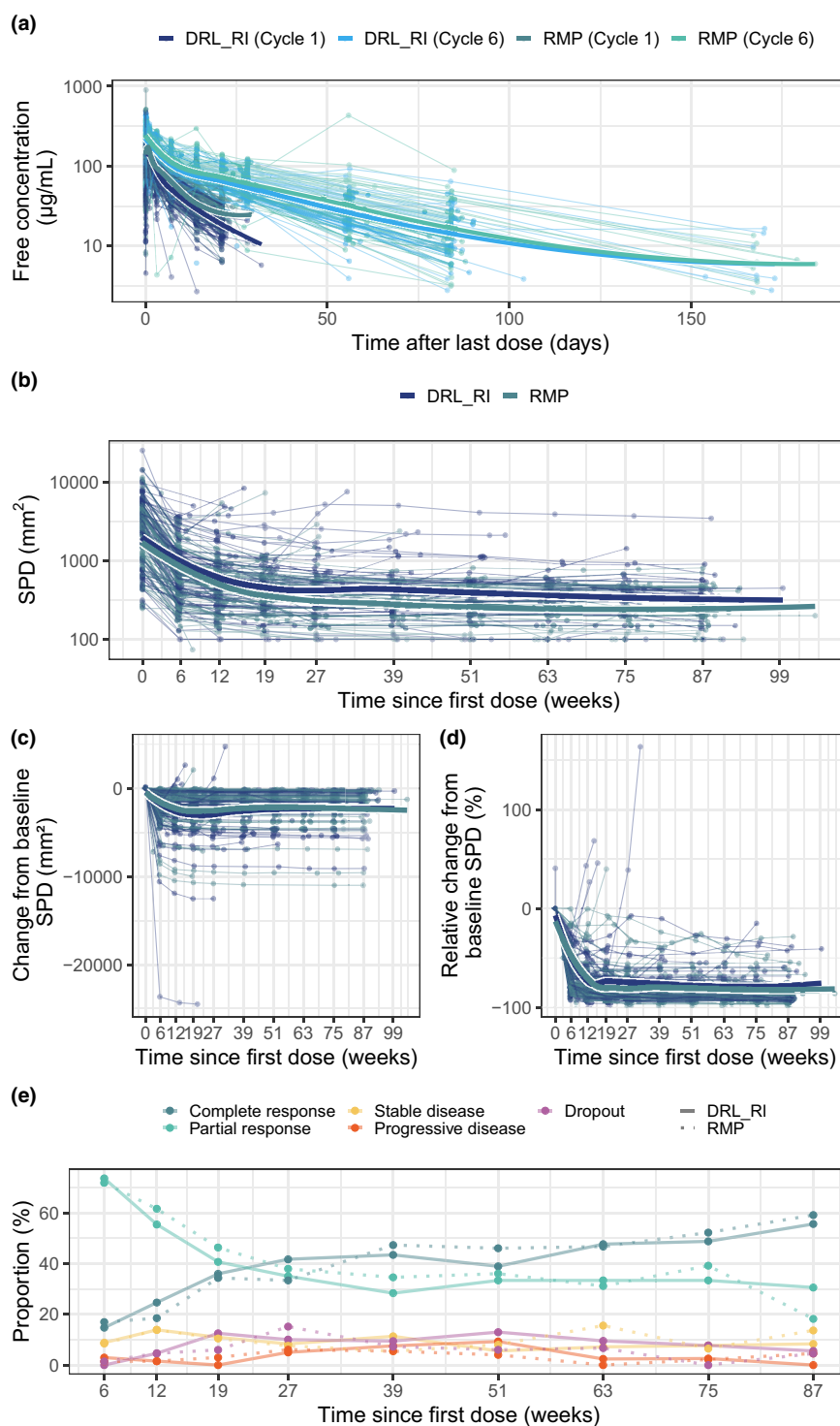
An overall gradual decrease of the tumor size over time was observed until a stable size was attained (Figure 1b). Although this trend was comparable between drug products, most patients with the highest tumor sizes over time were treated with DRL-RI. Nevertheless, the absolute and relative change from baseline tumor size was generally comparable between drug products (Figures 1c,d). This observation may be explained by the slightly larger baseline tumor size in patients randomly selected in the DRL-RI treatment arm (SPD in Table S2).

When considering tumor response during the study period, the proportion of patients in each response category, as well as the category transitions, were comparable between drug products (Figure 1e). The probability for a patient to transition to a different response category appeared to be time dependent. Specifically, at Week 6 (the first scheduled on-treatment tumor response assessment) most patients had transitioned from SD (assumed as the state of all patients prior to rituximab administration) to PR and then from PR to CR between Weeks 12 and 39. From about Week 39 onward, most patients remained in the same response category.

### Intermediate PK model

The final intermediate PK model was a TMDD model<sup>15</sup> with a QE assumption<sup>16</sup>: a two-compartment disposition model

**FIGURE 1** End point-specific graphical exploration. (a) Observed free rituximab plasma concentrations versus time after last dose, colored by drug product and treatment cycle in the analysis data set for the pharmacokinetic model. The plot includes data after Cycles 1 and 6. Each line represents data for one patient. The thicker lines are loess smooths. Measurements below the lower limit of quantification are not included in the plot. (b) Observed tumor size, measured as SPD, versus time on a semilogarithmic scale; data are colored by drug product in the analysis data set for the tumor size model. Each line represents data for one patient. (c) The same data shown in plot b but presented as change from baseline. (d) The same data shown in plot b but presented as relative change from baseline. (e) Proportion of patients in the observed tumor response categories, or dropout, for patients remaining in the study at the previous observation time; these proportions are plotted versus time since first dose for the analysis data set for the tumor response model, stratified by drug product and colored by tumor response category. Only observations from visits with scheduled tumor response assessments (thus not unscheduled visits) are included in the plot. DRL\_RI, Dr. Reddy's Laboratories rituximab; RMP, reference medicinal product; SPD, sum of products of diameters.



with two CL terms, one for the free drug and one for the drug-receptor complex ( $\text{CL}_{\text{complex}}$ ). The structural covariates included were drug product and WT, the latter considered as an allometric scaling factor on clearance and volume of distribution terms; among the exploratory covariates, sex was included on  $V_c$  because  $V_c$  was found to be lower for females, as previously reported.<sup>12</sup> IIV terms were included for  $V_c$ ,  $Q$ , and  $R_{\text{tot},0}$ , and a shared IIV was included on CL and  $\text{CL}_{\text{complex}}$ .

VPCs of drug concentrations over time (Figure S2a) and concentrations of trough samples (Figure S2b) as

well as parameter estimates (Table S4) are included as Supplementary Material. Altogether, these indicate an overall good description of the observed data and that parameters were estimated with reasonable precision by the final intermediate PK model despite the rather high RSE of  $\text{CL}_{\text{complex}}$  (50.7%; Table S4).

Five patients had at least one positive sample for ADA at any timepoint during the study. As a sensitivity analysis, the final intermediate PK model was reestimated after excluding ADA-positive subjects, which did not lead to

relevant differences in the final parameter estimates. In addition, the IIVs of the ADA-positive subjects were well within the IIV distributions of all subjects.

## Tumor size model

The final tumor size model (Equation 1) was a mixture model accounting for two subpopulations with different tumor regrowth rates (12.9% of the patients had a  $k_g$  of 0.133/week) and included a constant tumor kill rate for all patients, that is, no significant rituximab exposure–response relationship was included. None of the covariates tested by SCM, including drug product, was found to be significant for this model; thus, time-varying NTARG was the only structural covariate added (Equation 3). IIVs were included on  $TUM_0$ ,  $k_{kill}$ , Base,  $k_g$ , and  $\theta_{TUM, resistant}$ .

The parameters of the final model show reasonably precise parameter estimations (Table 1) despite the high RSE for the IIV in  $k_g$  (56.6%). Furthermore, a VPC showing SPD versus time since first tumor size measurement

(Figure S3) showed that the final model describes the data overall well.

## Tumor size–PK model

Tumor size effect on PK was then explored (Model S2, Figure 2). Two additional parameters were considered but did not modify the current model:  $SP_{drug\ product}$  (describing the relative difference between drug products in terms of dose reaching the system) and B-cell counts. Because  $SP_{drug\ product}$  was included to scale rituximab dose in the final intermediate PK model, its effect was retested here using SCM but was not found to be significant. Finally, the observed peripheral blood B-cell counts were tested as a structural covariate on CL (on top of tumor size) but not taken further.

Therefore, the final tumor size–PK model included the following components for CL:

$$CL(t) = CL + CL_{TS} \cdot e^{\theta \cdot \ln\left(\frac{TUM(t)}{TUM_{ref}}\right)}, \quad (6)$$

**TABLE 1** Parameter estimates of the final tumor size model

		Final tumor size model	
Run		21	
OFV		−1705.73	
Condition number		20.83	
	Unit	Value	RSE (%)
$TUM_0$	mm <sup>2</sup>	1830	10.4
$k_{kill}$	/week	0.322	8.55
$\theta_{Base}^a$	mm <sup>2</sup>	313	3.74
$\theta_{NTARG-base}$		1.06	3.16
$k_g^b$	/week	0.133	12.5
$\theta_{TUM, resistant}^c$	(logit scale)	−4.04	7.84
$p_{mix}$		0.871	3.91
IIV $TUM_0$	CV	1.08	7.78
IIV $k_{kill}$	CV	0.608	6.92
IIV Base	CV	0.124	15.0
IIV $k_g$	CV	0.336	56.6
IIV $\theta_{TUM, resistant}$	(STD, logit scale)	2.10	12.8
RUV	CV	0.126	1.82

Note: The RSE for IIV and RUV parameters are reported on the approximate STD scale. The MATRIX = S option was used to obtain the RSEs.

Abbreviations:  $\theta_{NTARG-base}$ , coefficient for number of target lesions on Base; CV, coefficient of variation; IIV, interindividual variability;  $k_g$ , first-order tumor growth rate constant;  $k_{kill}$ , first-order kill rate constant; OFV, objective function value;  $p_{mix}$ , probability to not have regrowth pattern; RSE, relative standard error; RUV, residual unexplained variability; STD, standard deviation; SHR, shrinkage;  $TUM_0$ , tumor size at baseline.

<sup>a</sup> $\theta_{Base}$  is a parameter representing the normal/healthy size of the target lymph nodes (for a subject with three target nodes/lesions) and describes the general tumor size level during follow-up in the present patient population. The specific tumor size during follow-up was given by Equation (3), where NTARG is the number of target lesions.

<sup>b</sup> $k_g$  is the growth rate for subjects with regrowth pattern (the probability to have regrowth pattern is  $1 - p_{mix}$ ).  $k_g$  was set to 0 for subjects without regrowth pattern (the probability to not have regrowth pattern is  $p_{mix}$ ).

<sup>c</sup> $\theta_{TUM, resistant}$  was estimated on the logit scale and corresponds to a fraction of resistant tumor burden of 1.73%.

where  $TUM(t)$  is the predicted tumor size at time  $t$ , and  $TUM_{ref}$  is the typical predicted tumor size at baseline.

The parameters of the final model show an overall low parameter uncertainty (Table 2). VPCs for this model were examined based on time since last dose for the complete time-course (Figure S4a), and for trough samples (Figure S4b). According to these, the final tumor size-PK model overall described the observed data well. However,

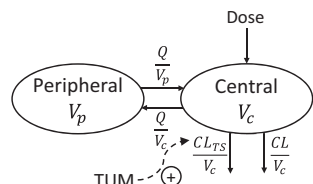


**FIGURE 2** Schematic representation of the tumor size-pharmacokinetic model. CL, clearance;  $V_c$ , central volume of distribution;  $Q$ , intercompartmental clearance;  $V_p$ , peripheral volume of distribution;  $CL_{TS}$ , tumor size-dependent CL; TUM, individually predicted tumor size.

for most cycles, a slight underprediction was observed in the trough samples for the RMP arm (Figure S4b).

## Tumor response model

The final model for tumor response (Table 3) was a CTMM with five states, that is, CR, PR, SD, PD, and DO (Figure 3, Model S3) and with no IIV included. TSFD was included as a structural covariate on the SD-PD and PR-CR transitions.  $TUM_0$  was a significant predictor for both  $k_{SD-PR,TSFD}$  and  $k_{SD-PD}$ : larger  $TUM_0$  predicted faster transitions between these states. Conversely, drug product was not a significant covariate on any parameter.

A relevant characteristic of this model is that it consists of a mixture model (with subpopulations of responders/nonresponders to treatment) with regard to all transitions to a worse state (Figure 3). Approximately 42% of patients was estimated to have some form of progression.

VPCs for the time course of observed tumor response categories (Figure S5) and the transitions between

**TABLE 2** Parameter estimates of the final tumor size-PK model

			Final tumor size-PK model	
Run			57	
OFV			-4816.60	
Condition number			27.59	
	Unit	Value	RSE (%)	SHR (%)
CL	L/h	0.0100	5.84	
$V_c$	L	3.87	3.46	
$Q$	L/h	0.0226	7.58	
$V_p$	L	5.45	2.67	
WT <sup>a</sup> on CL and $Q^b$		0.399	29.8	
WT <sup>a</sup> on $V_c$ and $V_p$		0.414	11.5	
Sex on $V_c^c$		-0.146	31.9	
$CL_{TS}$	L/h	0.00310	18.4	
Tumor size on $CL_{TS}^d$		1.06	8.06	
IIV CL	CV	0.297	8.80	12.3
IIV $V_c$	CV	0.254	5.01	6.78
IIV $Q$	CV	0.506	7.41	23.0
IIV on $CL_{TS}$	CV	1.40	12.2	24.2
RUV	CV	0.286	0.323	5.57

Note: The RSE for IIV and RUV parameters are reported on the approximate standard deviation scale. The MATRIX = S option was used to obtain the RSEs. Abbreviations: CL, clearance;  $CL_{TS}$ , tumor size-dependent CL; CV, coefficient of variation; IIV, interindividual variability; OFV, objective function value;  $Q$ , intercompartmental clearance; RSE, relative standard error; RUV, residual unexplained variability; SHR, shrinkage;  $V_c$ , central volume of distribution;  $V_p$ , peripheral volume of distribution; WT, body weight.

<sup>a</sup>WT was included on clearances and volumes of distribution using a power relationship with  $WT_{ref} = 75$  kg used as reference.

<sup>b</sup>Allometric scaling was included only on CL, not on the  $CL_{TS}$  component.

<sup>c</sup>Sex was included on  $V_c$ , with  $V_c$  being the typical value for a male subject ( $\theta_{Vc}$ ) and being an estimated value for females  $V_c = (\theta_{Vc} * [1 + \theta_{sex}])$ .

<sup>d</sup>Tumor size was included on  $CL_{TS}$  using a power relationship.



different tumor response categories confirmed that the final PK–pharmacodynamic model for tumor response provided an adequate description of the observed data.

### Simulations to visualize the impact of baseline tumor size on rituximab PK

The simulated PK profiles showed a moderate difference in rituximab PK: larger baseline tumor size resulted in lower rituximab exposure and higher drop-out (not shown). This was also reflected in the trends observed for the simulated  $AUC_{0-21}$  and  $C_{tr}$  (Figure 4 and Figure S6), whereas for the simulated  $C_{max}$  the differences between baseline tumor size scenarios were negligible.

## DISCUSSION

The population PK and PK–pharmacodynamic profiles of the two rituximab products (DRL\_RI and RMP) were characterized with the aims of identifying potential differences between drug products and assessing the impact of these differences on the demonstration of PK similarity. Once accounting for the population features, drug product was not a significant predictor of PK, change in tumor size, or tumor response.

In this analysis, we initially developed separate models for PK, tumor size, and tumor response, using data from study RI-01-002, conducted in 151 patients with DLBCL. All models described the data reasonably well, and drug products appeared comparable. No strong signs of TMDD were observed in the initial graphical analysis

**TABLE 3** Parameter estimates of the final model for tumor response

		Final tumor response model	
Run		136	
OFV		1595.46	
Condition number		13.22	
	Unit	Value	RSE (%)
$k_{SD-PR}$	/week	0.0500	23.6
Scaling factor $k_{SD-PR,TSFD}$ from $k_{SD-PR}$ <sup>a</sup>	/week	1000	(FIX)
$k_{PR-CR}$	/week	0.00766	39.4
$k_{PR-CR,TSFD}$	/week	0.0307	36.4
$k_{decay,SD-PR}$	/week	1.83	39.0
$k_{decay,PR-CR}$	/week	0.0526	41.7
$P_{resp}$		0.576	10.0
$k_{CR-PR}$	/week	0	(FIX)
$k_{CR-PR,prog}$	/week	0.0200	31.0
$k_{PR-SD}$	/week	0.00436	43.3
$k_{PR-SD,prog}$	/week	0.0652	22.2
$k_{SD-PD}$	/week	0	(FIX)
$k_{SD-PD,prog}$	/week	0.0550	27.8
$k_{CR-DO}$	/week	0.00284	32.9
$k_{PR-DO}$	/week	0.00514	23.3
$k_{SD-DO}$	/week	0.00754	45.7
$TUM_0$ on $k_{SD-PD}$		1.64	23.2
$TUM_0$ on $k_{SD-PR,TSFD}$		1.71	20.9

Note: The RSE for IIV and RUV parameters are reported on the approximate STD scale. RSE of parameter estimates was derived using the MATRIX = R option in NONMEM.

Abbreviations: CR, complete response; DO, dropout from tumor response assessment;  $k_{decay,i-j}$ , first-order exponential decay rate constant for the time since first dose effect on the transition from tumor response category  $i$  to  $j$ ;  $k_{i-j}$ , first-order transfer rate constant from tumor response category  $i$  to  $j$ ;  $k_{i-j,prog}$ , first-order transfer rate constant from tumor response category  $i$  to  $j$  for subpopulation with progression;  $k_{i-j,TSFD}$ , first-order transfer rate constant from tumor response category  $i$  to  $j$  that decays with time after first dose; OFV, objective function value; PD, progressive disease;  $P_{PD-DO}$ , probability of transition from progressive disease to dropout; PR, partial response;  $P_{resp}$ , proportion of population with slower transitions to clinically worse states; RSE, relative standard error; SD, stable disease; TSFD, time since first dose;  $TUM_0$ , baseline tumor size.

<sup>a</sup> $k_{SD-PR,TSFD} = 1000 * k_{SD-PR}$ ; the scaling factor of 1000 was determined using log-likelihood profiling.

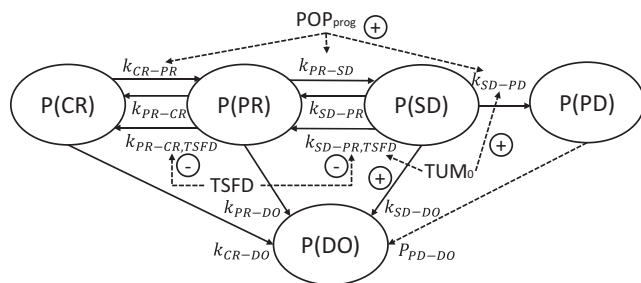


**FIGURE 3** Schematic representation of the final population pharmacokinetic–pharmacodynamic model for tumor response. Solid lines represent mass balance relationships, whereas dashed lines correspond to functional relationships. The definitions of the tumor response categories follow the Cheson et al 2007 criteria.<sup>25</sup> CR, complete response; DO, dropout from tumor response assessment;  $k_{i-j}$ , first-order transfer rate constant from tumor response category  $i$  to  $j$ ;  $k_{i-j,TSFD}$ , first-order transfer rate constant from tumor response category  $i$  to  $j$  that decays with time since first dose;  $P(i)$ , probability of tumor response category  $i$ ; PR, partial response;  $POP_{prog}$ , subpopulation with faster transitions to clinically worse states;  $P_{PD-DO}$ , probability of transition from progressive disease to dropout; PD, progressive disease; SD, stable disease; TSFD, time since first dose;  $TUM_0$ , baseline tumor size.

conducted to guide modeling, and this observation contrasts a previous publication reporting that rituximab undergoes TMDD.<sup>12</sup> At high rituximab concentrations, protein catabolism is the dominant CL pathway, and the CL becomes apparently linear due to target saturation. The inflection point characteristic of TMDD is often observable at low exposure, for example, at a longer time after the last dose. Noteworthy, lower dose levels, which are associated with lower rituximab exposure, were not considered; a single dose level (the approved dose for DLBCL) was tested in this study. A sensitivity analysis ruled out an effect of ADA positivity on the PK results. The final intermediate PK model included drug product as a dose-scaling parameter predicting 6.75% higher doses in RMP-treated patients. This initially suggested that different drug products may determine different rituximab exposures. However, when developing the tumor size–PK model, after tumor size was included as a predictor for rituximab CL, the drug product was not a significant covariate anymore. This indicated that the drug product effect on rituximab exposure detected earlier may not be a true difference but, rather, a consequence of different baseline and/or time-varying tumor sizes. The final tumor size–PK model indicated that patients with larger tumor size have higher total CL; based on the final parameter estimates, the contribution of tumor size–dependent CL to the total CL was approximately 24%.

The final tumor size–PK model was then used to perform simulations aimed at exploring the impact

of differences in baseline tumor size. The simulations showed that higher baseline tumor size is associated with slightly lower rituximab exposure and a higher dropout rate (Figure 4). Although in these simulations the difference in exposure does not seem to be clinically relevant, such a difference may complicate the demonstration of PK similarity; that is, the actual difference may be larger than that shown due to the association of larger baseline tumor size and higher probability to dropout. Therefore, differences in baseline tumor size between patients randomly assigned in the DRL\_RI and RMP arms (Figure 1b) may explain the slight difference in rituximab exposure between products (Figures S4).

The final tumor size model had a structure similar to that of a tumor growth model for solid tumors<sup>18</sup> but was adapted to reflect the DLBCL characteristics. In DLBCL, a criterion for complete response is the lymph node returning to normal size (rather than a complete tumor shrinkage, which can be observed in solid tumors). Tumors consisted of two fractions: one susceptible to treatment and one resistant to treatment.<sup>18</sup> The resistant fraction of the tumor was able to regrow, causing relapse/progressive disease. A mixture model predicted this regrowth to occur in a minority of patients (12.9%), whereas no regrowth was predicted in the remaining patients.

The sample size of the current study was chosen to demonstrate PK equivalence. Although this sample size seems sufficient for modeling continuous outcomes, such as PK and tumor size, it may not necessarily be adequate for modeling tumor response, which is an ordered categorical end point. In addition, the lack of both PK data for the CHOP components and an additional treatment arm using CHOP only limits our understanding of how much rituximab, on top of CHOP, contributes to changes in tumor size and tumor response. A relevant proportion of treated DLBCL patients are cured with CHOP therapy.<sup>33</sup> A major clinical trial in patients aged older than 60 years showed complete response rates of 63% with CHOP alone and 76% with the addition of rituximab.<sup>34</sup> Also, a study in younger patients,<sup>35</sup> closer to the age characteristics of this study, reported a 59% 3-year event-free survival with CHOP-like chemotherapies, which increased to 79% by adding rituximab. Thus, rituximab is considered a contributor to the already effective treatment. Altogether, this may contribute to explain why exposure–response relationships for tumor size and tumor response were not identified in our analysis. In addition, the single-dose level tested might have resulted in rituximab concentrations close to, or beyond, the saturation point for effect (where further increases in the rituximab concentrations do not result in a higher response), contributing to this lack of exposure–response relationship.

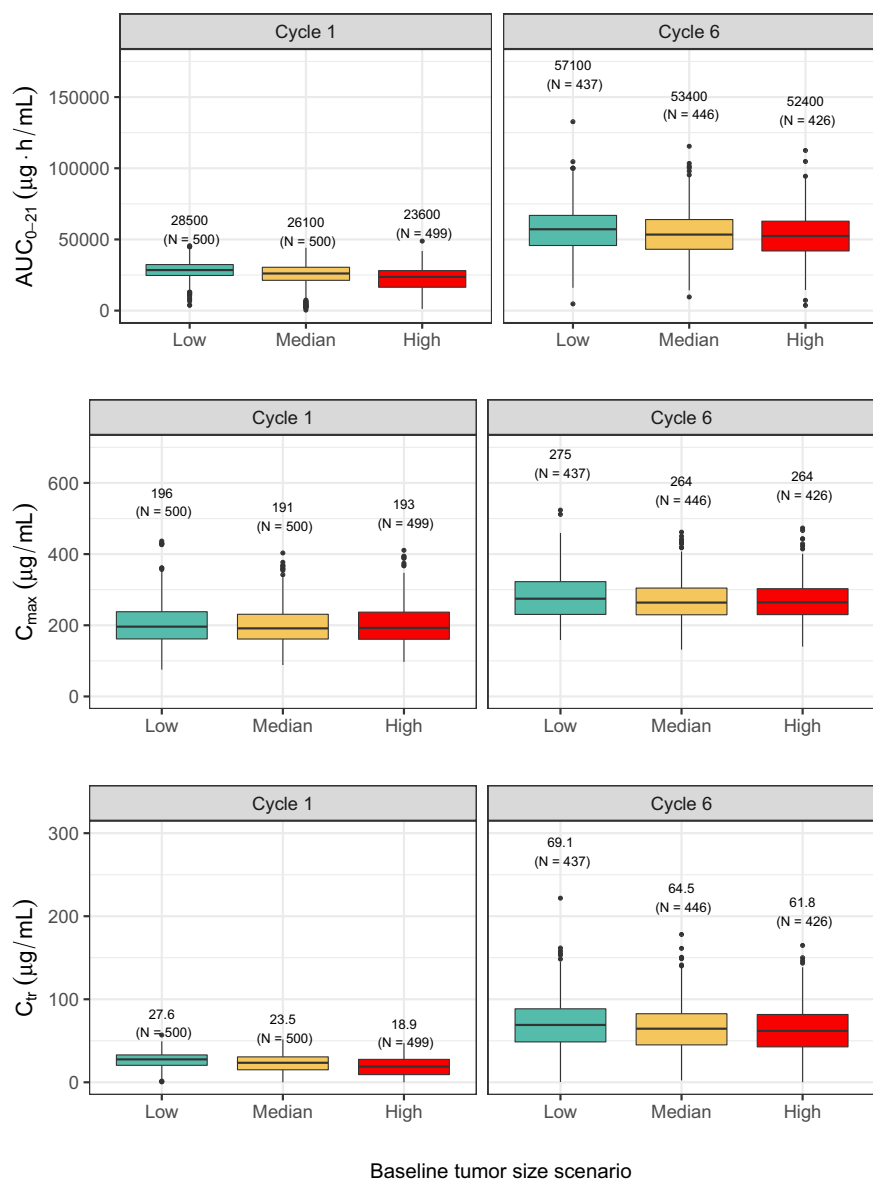


**FIGURE 4** Boxplot of simulated pharmacokinetic metrics for the low, median, and high baseline tumor size scenarios, stratified by treatment cycle. The horizontal line within each box represents the median; the box edges represent the 25th and 75th percentiles; the whiskers extend to the furthest data point that is no greater than 1.5 times the interquartile range. Each scenario was based on 500 simulated subjects. The median of pharmacokinetic metrics and number of patients contributing to each boxplot is shown above each box. Low, tumor size = 1070 mm<sup>2</sup>; median, tumor size = 2615 mm<sup>2</sup>; high, tumor size = 4681 mm<sup>2</sup>. AUC<sub>0-21</sub>, area under the curve over the dosing interval; C<sub>max</sub>, maximum concentration; C<sub>tr</sub>, trough concentration; N, number of patients.

The majority of SD–PR and PR–CR transitions occurred at early timepoints during treatment (Figure 1e). This suggests a time dependency of the drug effects and/or that a more susceptible part of the tumor is initially affected by treatment and a more resistant cell population may remain or arise due to the loss of CD20 expression at later times.<sup>4,5,36</sup> The TSFD effect was accounted for using an empirical exponential decay model. Because the decay half-life of  $k_{\text{decay,SD-PR}}$  is 0.379 weeks and that of  $k_{\text{decay,PR-CR}}$  is 13.2 weeks, the initial drug effect on the SD–PR transition decays much more rapidly than the initial drug effect on the PR–CR transition. Similar to the tumor size model, the final tumor response model describes a subpopulation of nonresponders to treatment (42% of the patients) with faster transitions to a worse state compared with the subpopulation of responders. DLBCL is a condition known to have a higher CD20 expression than other B-cell

malignancies. The subpopulation of nonresponders may correspond to patients who develop rituximab resistance over time; this may be attributable to therapy-induced loss of CD20 expression and/or selection of malignant B-cell clones with lower cell-surface CD20 expression.<sup>4,5,36</sup> Finally, larger baseline tumor size was found to be associated with faster SD–PR transitions right after the first rituximab administration and also faster SD–PD transitions in general.

This analysis presents additional limitations. First, the age limit for inclusion in the current study is 60 years, which is slightly lower than the median age of DLBCL diagnosis (64 years).<sup>37</sup> This determines a left-skewed age distribution in our study (Table S2) and limits the conclusions one can draw for older patients. By comparison, in the study by Rozman et al.<sup>12</sup> in which patients had an age range of 48–84 years and 58.6% of patients were aged >60 years,

age was found to be a significant covariate for linear, non-specific CL. However, in the study by Candelaria et al.,<sup>14</sup> using an upper age cap at 65 years, age was not a significant covariate, as in our study. Of note, the small sample size in the study by Rozman et al. ( $n = 29$ )<sup>12</sup> compared with the current study ( $n = 151$ ) and the study by Candelaria et al. ( $n = 251$ ),<sup>14</sup> as well as the different demographics observed, may limit effective comparison among these studies. The allometric exponents we estimated for clearances and volumes of distribution were smaller than the theoretical values of, respectively,  $\frac{3}{4}$  and 1. This difference is attributed to two factors: first, rituximab being a monoclonal antibody, which is frequently reported to have allometric exponent estimates that differ from the theoretical values;<sup>38</sup> and second, the narrow WT range in the current study in adults, which is often associated with allometric exponents being slightly underestimated.<sup>39–42</sup>

Another possible limitation of this study is that tumor size is based on computed tomography (CT) evaluation (i.e., anatomical) and not on the joint metabolic–anatomical evaluation awarded by positron emission tomography CT.<sup>25</sup> Despite this data limitation, the model works well, and the coefficient of variation of RUV was only 12.6%. The current analysis does not include genomic or proteomic features of the tumors. Also, the analysis considered the influence of tumor size on PK, whereas the reciprocal dependence of PK and tumor size was not accounted for. The final tumor size–PK model shows that responding patients undergoing tumor shrinkage will have increasing rituximab exposure, and nonresponding patients with tumor growth tend to have lower rituximab exposure. Finally, our analyses appear to differ from those shown by Viswabandya et al.,<sup>10</sup> who reported larger differences in PK metrics for DRL\_RI versus RMP for Cycle 6 compared with Cycle 1, despite confidence intervals broadly overlapping. It is worth noting that the comparison made is based on the population simulations generated based on the final tumor size–PK model, whereas the PK metrics reported by Viswabandya et al.<sup>10</sup> are based on noncompartmental analysis of individual-level, observed PK profiles. Population analysis allows including some patients whose  $AUC_{0-21}$  cannot be calculated using noncompartmental analysis; therefore, these analyses do not refer to the exact same population, which may determine other differences. In addition, it is worth noting that the reported 90% confidence intervals are largely overlapping between Cycle 1 and Cycle 6, suggesting that the difference may not be statistically significant. Using PK and PK–pharmacodynamic analyses, we found that a larger tumor size was associated with slightly lower rituximab exposure. No significant difference was found between drug products in PK, tumor size change, or tumor response. The current study exemplifies how PK and

PK–pharmacodynamic analyses can be applied to identify hidden factors generating apparent differences between drug products, therefore contributing to PK similarity assessment.

## AUTHOR CONTRIBUTIONS

R.J.S. and Q.X.O. designed and performed the research, analyzed the data, and wrote the manuscript. N.M. and P.K.R. wrote the manuscript. L.E.F., L.L.L., and E.H. designed the research, analyzed the data, and wrote the manuscript.

## ACKNOWLEDGMENTS

The authors thank Viviana Moroso, PhD, of Pharmetheus AB (Uppsala, Sweden), for providing medical writing support, which was funded by Dr. Reddy's Laboratories Ltd (Hyderabad, India) in accordance with Good Publication Practice (GPP3) guidelines (<http://www.ismpp.org/gpp3>). The authors also thank Sidharth Bichpuria, M. Tech, Senior Scientist at Pre-Clinical Development (Dr. Reddy's Laboratories Ltd, Hyderabad, India) and Vikas Kumar, PhD, Head of Pre-Clinical Development (Dr. Reddy's Laboratories Ltd, Hyderabad, India), for contributing to the development of the bioanalytical methods used to determine the concentrations of rituximab and antirrituximab antibodies and for summarizing the bioanalytical methods for inclusion in the article.

## FUNDING INFORMATION

This work was supported by Dr. Reddy's Laboratories (study number: RI-01-002 [Clinical Trials Registry - India//2012/11/003129]).

## CONFLICT OF INTEREST

R.J.S. was a Pharmetheus AB employee at the time of conducting the work. Q.X.O. and E.H. are Pharmetheus AB employees. L.E.F. is a Pharmetheus AB paid consultant and shareholder. N.M. and L.L.L. are Dr. Reddy's Laboratories employees and shareholders. P.K.R. is a Dr. Reddy's Laboratories employee. Support for R.J.S., Q.X.O., L.E.F., and E.H. at Pharmetheus AB was contracted and funded by Dr. Reddy's Laboratories.


## DISCLAIMER

As Deputy Editor-in-Chief of *Pharmacometrics & Systems Pharmacology*, Lena E. Friberg was not involved in the review or decision process for this article.

## ORCID

Qing Xi Ooi  <https://orcid.org/0000-0003-4310-9842>

Lena E. Friberg  <https://orcid.org/0000-0002-2979-679X>

Luis López-Lázaro  <https://orcid.org/0000-0003-0620-6133>

## REFERENCES

- Plosker GL, Figgitt DP. Rituximab: a review of its use in non-Hodgkin's lymphoma and chronic lymphocytic Leukaemia. *Drugs*. 2003;63:803-843.
- Molina A. A decade of rituximab: improving survival outcomes in non-Hodgkin's lymphoma. *Annu Rev Med*. 2008;59:237-250.
- Stewart Bernard W, Wild C. International agency for research on cancer, & world health organization. *World Cancer Report*. 2014;2014:490.
- Olejniczak SH, Stewart CC, Donohue K, Czuczman MS. A quantitative exploration of surface antigen expression in common B-cell malignancies using flow cytometry. *Immunol Investig*. 2006;35:93-114.
- Prevodnik VK, Lavrenčak J, Horvat M, Novaković BJ. The predictive significance of CD20 expression in B-cell lymphomas. *Diagn Pathol*. 2011;6:33.
- Chaganti S, Illidge T, Barrington S, et al. Guidelines for the management of diffuse large B-cell lymphoma. *Br J Haematol*. 2016;174:43-56.
- Zelenetz AD, Gordon LI, Wierda WG, et al. Non-Hodgkin's lymphomas, version 4.2014. *J Natl Compr Cancer Netw*. 2014;12:1282-1303.
- Buske C, Ogura M, Kwon H-C, Yoon SW. An introduction to biosimilar cancer therapeutics: definitions, rationale for development and regulatory requirements. *Future Oncol*. 2017;13:5-16.
- Chopra R, Lopes G. Improving access to cancer treatments: the role of Biosimilars. *J Glob Oncol*. 2017;3:596-610.
- Viswabandya A, Shah S, Mukhopadhyay A, et al. Randomized, double-blind, pharmacokinetic equivalence trial comparing DRL-rituximab with MabThera in patients with diffuse large B-cell lymphoma. *JGO*. 2019;5:1-13. doi:10.1200/JGO.19.00248
- Haridas VM, Katta R, Nalawade A, et al. Pharmacokinetic similarity and comparative pharmacodynamics, safety, efficacy, and immunogenicity of DRL\_RI versus reference rituximab in biologics-Naïve patients with moderate-to-severe rheumatoid arthritis: a double-blind, randomized, Three-Arm Study. *BioDrugs*. 2020;34:183-196.
- Rozman S, Grabnar I, Novaković S, Mrhar A, Jezeršek Novaković B. Population pharmacokinetics of rituximab in patients with diffuse large B-cell lymphoma and association with clinical outcome. *Br J Clin Pharmacol*. 2017;83:1782-1790.
- Zhang L, Beal SL, Sheiner LB. Simultaneous vs. sequential analysis for population PK/PD data I: best-case performance. *J Pharmacokinet Pharmacodyn*. 2003;30:387-404.
- Candelaria M, Gonzalez D, Fernández Gómez FJ, et al. Comparative assessment of pharmacokinetics, and pharmacodynamics between RTX83™, a rituximab biosimilar, and rituximab in diffuse large B-cell lymphoma patients: a population PK model approach. *Cancer Chemother Pharmacol*. 2018;81:515-527.
- Jin F, Krzyzanski W. Pharmacokinetic model of target-mediated disposition of thrombopoietin. *AAPS J*. 2004;6:86-93.
- Mager DE, Krzyzanski W. Quasi-equilibrium pharmacokinetic model for drugs exhibiting target-mediated drug disposition. *Pharm Res*. 2005;22:1589-1596.
- Claret L, Girard P, Hoff PM, et al. Model-based prediction of phase III overall survival in colorectal cancer on the basis of phase II tumor dynamics. *JCO*. 2009;27:4103-4108.
- Stein WD, Yang J, Bates SE, Fojo T. Bevacizumab reduces the growth rate constants of renal carcinomas: a novel algorithm suggests early discontinuation of bevacizumab resulted in a lack of survival advantage. *Oncologist*. 2008;13:1055-1062.
- Karlsson MO, Schoemaker RC, Kemp B, et al. A pharmacodynamic Markov mixed-effect model for the effect of temazepam on sleep. *Clin Pharmacol Therap*. 2000;68:175-188.
- Bergstrand M, Söderlind E, Weitschies W, Karlsson M. Mechanistic modeling of a magnetic marker monitoring study linking gastrointestinal tablet transit, In vivo drug release, and pharmacokinetics. *Clin Pharmacol Therap*. 2009;86:77-83.
- Bergstrand M, Söderlind E, Eriksson UG, Weitschies W, Karlsson MO. A semi-mechanistic modeling strategy for characterization of regional absorption properties and prospective prediction of plasma concentrations following administration of new modified release formulations. *Pharm Res*. 2012;29:574-584.
- Hénin E, Bergstrand M, Standing JF, Karlsson MO. A mechanism-based approach for absorption modeling: the gastro-intestinal transit time (GITT) model. *AAPS J*. 2012;14:155-163.
- Pilla Reddy V, Petersson KJ, Suleiman AA, Vermeulen A, Proost JH, Friberg LE. Pharmacokinetic-pharmacodynamic modeling of severity levels of extrapyramidal side effects with markov elements. *CPT: PSP*. 2012;1:1.
- Lacroix BD, Karlsson MO, Friberg LE. Simultaneous exposure-response modeling of ACR20, ACR50, and ACR70 improvement scores in rheumatoid arthritis patients treated with certolizumab pegol. *CPT: PSP*. 2014;3:e143.
- Cheson BD, Pfistner B, Juweid ME, et al. Revised response criteria for malignant lymphoma. *JCO*. 2007;25:579-586.
- Lindbom L, Ribbing J, Jonsson EN. Perl-speaks-NONMEM (PsN) - a Perl module for NONMEM related programming. *Comput Methods Prog Biomed*. 2004;75:85-94.
- Lindbom L, Pihlgren P, Jonsson N. PsN-toolkit - a collection of computer intensive statistical methods for non-linear mixed effect modeling using NONMEM. *Comput Methods Prog Biomed*. 2005;79:241-257.
- Harling K, Ueckert S, Hooker AC, Jonsson EN, Karlsson MO. Xpose and Perl speaks NONMEM (PsN), PAGE 19. 2010. Abstr 1842. [www.page-meeting.org/?abstract=1842](http://www.page-meeting.org/?abstract=1842).
- Svensson RJ, Jonsson EN. Efficient and relevant stepwise covariate model building for pharmacometrics. *CPT Pharmacometrics Syst Pharmacol*. 2022;11:1210-1222. doi:10.1002/psp4.12838
- Beal SL, Sheiner LB, Boeckmann AJ, Bauer RJ. *NONMEM User's Guides. (1989-2014)*. Icon Development Solutions; 2014.
- R Development Core Team. *R: A Language and Environment for Statistical Computing. R Foundation for Statistical Computing*. R Development Core Team; 2007 ISBN 3-900051-07-0. <http://www.R-project.org>
- Jonsson EN, Karlsson MO. Xpose—an S-PLUS based population pharmacokinetic/pharmacodynamic model building aid for NONMEM. *Comput Methods Prog Biomed*. 1999;58:51-64.
- Maurer MJ, Habermann TM, Shi Q, et al. Progression-free survival at 24 months (PFS24) and subsequent outcome for patients with diffuse large B-cell lymphoma (DLBCL) enrolled on randomized clinical trials. *Ann Oncol*. 2018;29:1822-1827.
- Coiffier B, Lepage E, Brière J, et al. CHOP chemotherapy plus rituximab compared with CHOP alone in elderly patients with diffuse large-B-cell lymphoma. *N Engl J Med*. 2002;346:235-242.

35. Pfreundschuh M, Trümper L, Osterborg A, et al. CHOP-like chemotherapy plus rituximab versus CHOP-like chemotherapy alone in young patients with good-prognosis diffuse large-B-cell lymphoma: a randomised controlled trial by the MabThera international trial (MInT) group. *Lancet Oncol*. 2006;7:379-391.
36. Pavlasova G, Mraz M. The regulation and function of CD20: an “enigma” of B-cell biology and targeted therapy. *Haematologica*. 2020;105:1494-1506.
37. *Harrison's Principles of Internal Medicine*. McGraw-Hill Education; 2018.
38. Germovsek E, Cheng M, Giragossian C. Allometric scaling of therapeutic monoclonal antibodies in preclinical and clinical settings. *MAbs*. 2021;13:1964935.
39. Xu Y, Langevin BA, Zhou H, Xu Z. Model-aided adults-to-children pharmacokinetic extrapolation and empirical body size-based dosing exploration for therapeutic monoclonal antibodies—is Allometry a reasonable choice? *J Clin Pharmacol*. 2020;60:1573-1584.
40. Bai S, Jorga K, Xin Y, et al. A guide to rational dosing of monoclonal antibodies. *Clin Pharmacokinet*. 2012;51:119-135.
41. Zheng S, Gaitonde P, Andrew MA, Gibbs MA, Lesko LJ, Schmidt S. Model-based assessment of dosing strategies in children for monoclonal antibodies exhibiting target-mediated drug disposition. *CPT: Pharmacometrics & Systems Pharmacology*. 2014;3:138.
42. Yee KL, Kleijn HJ, Kerbusch T, et al. Population pharmacokinetics and pharmacodynamics of Bezlotoxumab in adults with primary and recurrent *Clostridium difficile* infection. *Antimicrob Agents Chemother*. 2019;63:e01971-e01918.

## SUPPORTING INFORMATION

Additional supporting information can be found online in the Supporting Information section at the end of this article.

**How to cite this article:** Svensson RJ, Ooi QX, Friberg LE, et al. Rituximab pharmacokinetic and pharmacokinetic–pharmacodynamic evaluation based on a study in diffuse large B-cell lymphoma: Influence of tumor size on pharmacokinetic and assessment of pharmacokinetic similarity. *CPT Pharmacometrics Syst Pharmacol*. 2023;12:154-167. doi: [10.1002/psp4.12885](https://doi.org/10.1002/psp4.12885)